PERGAMON

Atmospheric Environment 37 (2003) 5097–5114

ATMOSPHERIC ENVIRONMENT

www.elsevier.com/locate/atmosenv

Direct and adjoint sensitivity analysis of chemical kinetic systems with KPP: II—numerical validation and applications

Dacian N. Daescu[a], Adrian Sandu[b], Gregory R. Carmichael[c,*]

[a] *Institute for Mathematics and its Applications, University of Minnesota, 400 Lind Hall 207 Church Street S.E., Minneapolis, MN 55455, USA*

[b] *Department of Computer Science, Virginia Polytechnic Institute and State University, 660 McBryde Hall, Blacksburg, VA 24061, USA*

[c] *Center for Global and Regional Environmental Research, 204 IATL, The University of Iowa, Iowa City, IA 52242-1297, USA*

Received 26 January 2003; accepted 7 August 2003

Abstract

The Kinetic PreProcessor KPP was extended to generate the building blocks needed for the direct and adjoint sensitivity analysis of chemical kinetic systems. An overview of the theoretical aspects of sensitivity calculations and a discussion of the KPP software tools is presented in the companion paper.

In this work the correctness and efficiency of the KPP generated code for direct and adjoint sensitivity studies are analyzed through an extensive set of numerical experiments. Direct-decoupled Rosenbrock methods are shown to be cost-effective for providing sensitivities at low and medium accuracies. A validation of the discrete–adjoint evaluated gradients is performed against the finite difference estimates. The accuracy of the adjoint gradients is measured using a reference gradient value obtained with a standard direct-decoupled method. The accuracy is studied for both constant step size and variable step size integration of the forward/adjoint model and the consistency between the discrete and continuous adjoint models is analyzed.

Applications of the KPP-1.2 software package to direct and adjoint sensitivity studies, variational data assimilation, and parameter identification are considered for the comprehensive chemical mechanism SAPRC-99.

Keywords: Sensitivity analysis; Data assimilation; Parameter identification; Optimization

1. Introduction

The direct-decoupled method and the adjoint method are powerful tools for sensitivity analysis. Currently, several commercial software packages such as SENKIN (Lutz et al., 1987) and LSENS (Radhakrishnan, 2003) implement the direct-decoupled method for the sensitivity analysis of gas-phase chemical reactions. Given a chemical kinetics system described by a list of chemical reactions, the Kinetic PreProcessor KPP (Damian-Iordache et al., 2002) generates the FORTRAN 77 or C code for the forward model integration and subroutines that allow direct-decoupled/adjoint sensitivity analysis with minimal user intervention. The capability to implement the continuous/discrete adjoint sensitivity analysis represents a major contribution of the new release KPP-1.2.

An overview of the theoretical aspects of sensitivity calculations and a discussion of the KPP software tools is presented in the companion paper (Sandu et al., 2003). In this paper, we present an extensive set of numerical experiments and applications of the KPP software to sensitivity studies for chemical kinetics systems.

Our tests use the SAPRC-99 atmospheric chemistry mechanism (Carter, 2000a, b) which considers the gas-phase atmospheric reactions of volatile organic

*Corresponding author. Tel.: +1-319-335-3333; fax: +1-319-335-3337.

E-mail addresses: daescu@ima.umn.edu (D.N. Daescu), asandu@cs.vt.edu (A. Sandu), gcarmich@cgrer.uiowa.edu (G.R. Carmichael).

1352-2310/$ - see front matter
doi:10.1016/j.atmosenv.2003.08.020

compounds (VOCs) and nitrogen oxides (NO_x) in urban and regional settings. The chemical mechanism was developed at University of California, Riverside by Dr. W.P.L. Carter for use in airshed models for predicting the effects of VOC and NO_x emissions on tropospheric secondary pollutants formation such as ozone (O_3) and other oxidants. In our analysis we consider the condensed fixed-parameter version of the SAPRC-99 mechanism (Carter, 2000a) which is suitable for implementation into the Models-3 software framework. This version takes into consideration 211 reactions among 74 variable chemical species (in addition O2, H2, CH4, and H2O concentrations are considered fixed), and is currently incorporated into the three-dimensional regional-scale model STEM-II (Carmichael et al., 1986). A list of the variable chemical species in the model is presented in Table 1.

In Section 2 we present the numerical solvers available in the KPP library for direct-decoupled and discrete/continuous adjoint sensitivity calculations. Experimental settings, the forward model integration, and issues related to the sparse linear algebra computations are discussed. Direct sensitivity calculations with respect to initial conditions and to reaction rate coefficients using Rosenbrock solvers up to order four are presented in Section 3. The accuracy and the efficiency of the direct-decoupled method is analyzed. Section 4 is dedicated to adjoint sensitivity analysis. Adjoint model validation, consistency between the discrete and adjoint model, and accuracy issues are discussed. The computational expense and the efficiency of the adjoint model are investigated. Applications are presented for time-dependent sensitivities with respect to the model state, reaction rate coefficients, and emissions. In Section 5 we present applications of the adjoint modeling to variational data assimilation and parameter estimation using the initial conditions and emission rates as control variables. Concluding remarks and future research directions are presented in Section 6.

2. Numerical solvers

The dynamical model associated with the chemical mechanism is given by a system of nonlinear ordinary differential equations (ODEs)

$$\frac{dy}{dt} = f(y) + E, \tag{1}$$

where $y \in R^n$ is the vector of concentrations, $f(y)$ is the chemical production/loss function, and $E \in R^n$ represents the vector of emission rates ($E_i = 0$ if there are no emissions of species i). Throughout this paper an upper index will specify the discrete time moment and a lower index will specify the vector component. For example, y^i is the concentration vector at time t^i and y_j denotes the jth component of the vector y.

Due to the wide range of characteristic time scales of the chemical reactions, the eigenvalues of the Jacobian matrix $J = \partial f/\partial y$ may differ by several orders of magnitude. Such systems are usually referred to as being "stiff" (Aiken, 1985). Explicit numerical methods are usually impractical to integrate stiff systems since may exhibit a severe restriction of the step size. For this reason, numerical schemes that are particularly suitable for integrating stiff ODE systems have been developed (Aiken, 1985; Hairer and Wanner, 1991).

Rosenbrock methods (Hairer and Wanner, 1991) are well-suited for atmospheric chemistry applications (Sandu et al., 1997) due to their optimal stability properties and conservation of the linear invariants of the system (e.g. they are mass-conservative). When the sparsity of the ODE system is carefully exploited, Rosenbrock methods can efficiently integrate atmospheric chemistry systems. The accuracy requirements in atmospheric transport-chemistry models are modest (1%) such that low-order methods are usually employed. For the numerical experiments we consider the second-order two-stage L-stable solver ROS2 (Verwer et al., 1999) and the third-order four-stage stiffly accurate solver RODAS3 (Sandu et al., 1997). Both integrators use variable step size for error control and the forward, discrete, and continuous adjoint model integrations have been implemented using the KPP software tools. The derivation of the discrete adjoint formulae follows our previous work (Daescu et al., 2000). Two other methods presented by Hairer and Wanner (1991) are included in the KPP-1.2 numerical library: the linearly-implicit Euler method (one-stage Rosenbrock) implemented with constant step size is available in forward/adjoint mode for testing purposes only, and the fourth-order four-stage L-stable solver ROS4 is available for direct-decoupled sensitivity.

2.1. Experimental settings

For the numerical experiments we selected a pollution scenario with urban VOC and high NO_x levels using input data and reaction rate constants from Carter (2000a) MD3TEST2, as follows: the model simulation starts at local noon (t^s = 12:00LT) with the concentration of all variable chemical species set to zero. Emissions are prescribed at constant rates for 30 chemical species in the model as specified in Table 2 (E_i^{ref}). We assume a day time interval from 4:30LT (sunrise) to 19:30LT (sunset) with the photolysis reaction rates updated every 15 min, and a constant temperature of 300 K. The system is integrated for 24 h and the resulting state y^0 at $t^0 = t^s + 24$h is taken as the initial state of the model for a 5 day run (120 h). The

Table 1
Finite difference (FD), discrete adjoint (DADJ) and continuous adjoint (CADJ) evaluated gradients $\partial O_3(t^F)/\partial y_i^0$ using RODAS3 and ROS2 solvers with $h = 60$ s

KPP	Chemical	RODAS3			ROS2		
no.	species	FD	DADJ	CADJ	FD	DADJ	CADJ
1†	H2SO4	0.00000E+00	0.00000E+00	0.00000E+00	0.00000E+00	0.00000E+00	0.00000E+00
2†	HCOOH	0.00000E+00	0.00000E+00	0.00000E+00	0.00000E+00	0.00000E+00	0.00000E+00
3†	CCO_OH	0.00000E+00	0.00000E+00	0.00000E+00	0.00000E+00	0.00000E+00	0.00000E+00
4†	RCO_OH	0.00000E+00	0.00000E+00	0.00000E+00	0.00000E+00	0.00000E+00	0.00000E+00
5†	CCO_OOH	0.00000E+00	0.00000E+00	0.00000E+00	0.00000E+00	0.00000E+00	0.00000E+00
6†	RCO_OOH	0.00000E+00	0.00000E+00	0.00000E+00	0.00000E+00	0.00000E+00	0.00000E+00
7†	XN	0.00000E+00	0.00000E+00	0.00000E+00	0.00000E+00	0.00000E+00	0.00000E+00
8†	XC	0.00000E+00	0.00000E+00	0.00000E+00	0.00000E+00	0.00000E+00	0.00000E+00
9	SO2	0.13782E−02	0.13782E−02	0.13914E−02	0.13779E−02	0.13779E−02	0.13808E−02
10◇	O1D	0.39652E−02	0.39653E−02	0.39626E−02	0.39710E−02	0.39710E−02	0.39663E−02
11	ALK1	0.95137E−02	0.95138E−02	0.95762E−02	0.95135E−02	0.95136E−02	0.95512E−02
12	BACL	0.38263E−01	0.38264E−01	0.38252E−01	0.38265E−01	0.38265E−01	0.38234E−01
13	PAN	0.19317E+00	0.19317E+00	0.19292E+00	0.19317E+00	0.19317E+00	0.19299E+00
14	PAN2	0.21875E+00	0.21875E+00	0.21854E+00	0.21875E+00	0.21875E+00	0.21860E+00
15	PBZN	−0.12949E+00	−0.12949E+00	−0.12919E+00	−0.12949E+00	−0.12949E+00	−0.12929E+00
16	MA_PAN	0.21605E+00	0.21605E+00	0.21581E+00	0.21605E+00	0.21605E+00	0.21588E+00
17	H2O2	0.47951E−02	0.47951E−02	0.47927E−02	0.47951E−02	0.47951E−02	0.47909E−02
18	N2O5	0.34423E+00	0.34424E+00	0.34373E+00	0.34423E+00	0.34423E+00	0.34390E+00
19	HONO	0.17247E+00	0.17247E+00	0.17221E+00	0.17248E+00	0.17248E+00	0.17231E+00
20	ALK2	0.16202E−01	0.16202E−01	0.16297E−01	0.16202E−01	0.16202E−01	0.16254E−01
21	ALK3	0.31035E−01	0.31035E−01	0.31226E−01	0.31034E−01	0.31034E−01	0.31143E−01
22◇*	TBU_O	0.74430E−01	0.74434E−01	0.17916E−01	0.58709E−01	0.58702E−01	0.17881E−01
23	ALK5	0.54248E−01	0.54248E−01	0.54530E−01	0.54247E−01	0.54247E−01	0.54419E−01
24	ARO2	0.17430E−02	0.17433E−02	0.20331E−02	0.17424E−02	0.17427E−02	0.19140E−02
25	HNO4	0.17847E+00	0.17847E+00	0.17822E+00	0.17848E+00	0.17848E+00	0.17831E+00
26	COOH	0.68350E−02	0.68350E−02	0.68520E−02	0.68345E−02	0.68345E−02	0.68367E−02
27◇	HOCOO	0.13174E−01	0.13171E−01	0.13111E−01	0.13159E−01	0.13157E−01	0.13109E−01
28◇*	BZNO2_O	−0.59814E+00	−0.17698E+00	−0.17093E+00	−0.33906E+00	−0.19449E+00	−0.17102E+00
29	MEOH	0.60444E−03	0.60445E−03	0.63238E−03	0.60379E−03	0.60380E−03	0.60682E−03
30	ALK4	0.46236E−01	0.46237E−01	0.46447E−01	0.46236E−01	0.46236E−01	0.46357E−01
31	ARO1	−0.40153E−01	−0.40152E−01	−0.39826E−01	−0.40155E−01	−0.40154E−01	−0.39965E−01
32	DCB2	0.56868E−01	0.56868E−01	0.56921E−01	0.56871E−01	0.56871E−01	0.56885E−01
33	DCB3	0.55593E−01	0.55592E−01	0.55642E−01	0.55603E−01	0.55602E−01	0.55618E−01
34	CRES	−0.27493E+00	−0.27494E+00	−0.27433E+00	−0.27493E+00	−0.27494E+00	−0.27458E+00
35	DCB1	0.56370E−01	0.56370E−01	0.56510E−01	0.56372E−01	0.56372E−01	0.56456E−01
36	NPHE	−0.16736E+00	−0.16736E+00	−0.16700E+00	−0.16736E+00	−0.16736E+00	−0.16714E+00
37	ROOH	0.50228E−01	0.50228E−01	0.50325E−01	0.50228E−01	0.50228E−01	0.50284E−01
38	BALD	−0.23158E+00	−0.23158E+00	−0.23114E+00	−0.23158E+00	−0.23158E+00	−0.23128E+00
39	PHEN	−0.23380E+00	−0.23381E+00	−0.23328E+00	−0.23380E+00	−0.23381E+00	−0.23350E+00
40	CO	0.11600E−02	0.11600E−02	0.11622E−02	0.11599E−02	0.11599E−02	0.11579E−02
41	MGLY	0.22371E−01	0.22371E−01	0.22375E−01	0.22371E−01	0.22372E−01	0.22358E−01
42	ACET	0.37252E−02	0.37252E−02	0.37579E−02	0.37255E−02	0.37255E−02	0.37392E−02
43	HNO3	0.18192E+00	0.18192E+00	0.18180E+00	0.18192E+00	0.18192E+00	0.18182E+00
44	ETHENE	0.22913E−01	0.22913E−01	0.22979E−01	0.22912E−01	0.22912E−01	0.22947E−01
45	GLY	0.16976E−01	0.16976E−01	0.16985E−01	0.16975E−01	0.16975E−01	0.16971E−01
46◇	BZ_O	−0.33741E+00	−0.33742E+00	−0.33763E+00	−0.33759E+00	−0.33761E+00	−0.33787E+00
47	ISOPRENE	0.48924E−01	0.48925E−01	0.49140E−01	0.48929E−01	0.48929E−01	0.49060E−01
48◇	R2O2	0.29810E−02	0.29821E−02	0.29958E−02	0.29740E−02	0.29744E−02	0.29939E−02
49	TERP	0.21421E−01	0.21420E−01	0.21670E−01	0.21434E−01	0.21432E−01	0.21595E−01
50	METHACRO	0.42481E−01	0.42481E−01	0.42591E−01	0.42481E−01	0.42481E−01	0.42540E−01
51	OLE1	0.46460E−01	0.46460E−01	0.46606E−01	0.46461E−01	0.46461E−01	0.46547E−01
52	ISOPROD	0.53388E−01	0.53388E−01	0.53549E−01	0.53389E−01	0.53389E−01	0.53481E−01
53	OLE2	0.25213E−01	0.25213E−01	0.25340E−01	0.25215E−01	0.25215E−01	0.25286E−01
54	MVK	0.47508E−01	0.47508E−01	0.47585E−01	0.47508E−01	0.47509E−01	0.47540E−01

Table 1 (*continued*)

KPP	Chemical	RODAS3			ROS2		
no.	species	FD	DADJ	CADJ	FD	DADJ	CADJ
55	CCHO	0.15508E−01	0.15508E−01	0.15530E−01	0.15509E−01	0.15509E−01	0.15513E−01
56	HCHO	0.58214E−02	0.58214E−02	0.58295E−02	0.58211E−02	0.58211E−02	0.58217E−02
57	RNO3	0.15063E+00	0.15063E+00	0.15074E+00	0.15063E+00	0.15063E+00	0.15069E+00
58◇*	O3P	0.78351E−02	0.78358E−02	0.33817E−02	0.66128E−02	0.66127E−02	0.33817E−02
59	RCHO	0.41519E−01	0.41519E−01	0.41589E−01	0.41520E−01	0.41520E−01	0.41555E−01
60	MEK	0.33771E−01	0.33771E−01	0.33925E−01	0.33771E−01	0.33771E−01	0.33856E−01
61	PROD2	0.63755E−01	0.63755E−01	0.63953E−01	0.63754E−01	0.63755E−01	0.63871E−01
62	O3	0.33846E−02	0.33846E−02	0.33820E−02	0.33845E−02	0.33845E−02	0.33820E−02
63◇*	HO2	0.72890E−02	0.72897E−02	0.72830E−02	0.72946E−02	0.72939E−02	0.72881E−02
64◇*	RO2_N	−0.44712E−02	−0.44706E−02	−0.42890E−02	−0.42812E−02	−0.42823E−02	−0.43715E−02
65◇*	MA_RCO3	0.42230E−01	0.42230E−01	0.42726E−01	0.42313E−01	0.42313E−01	0.42711E−01
66◇	C_O2	0.14321E−01	0.14331E−01	0.14347E−01	0.14283E−01	0.14286E−01	0.14331E−01
67◇*	BZCO_O2	−0.29611E+00	−0.29611E+00	−0.29996E+00	−0.29701E+00	−0.29702E+00	−0.30014E+00
68◇	RO2_R	0.16698E−01	0.16644E−01	0.16608E−01	0.16755E−01	0.16727E−01	0.16619E−01
69	NO	0.16740E+00	0.16740E+00	0.16715E+00	0.16740E+00	0.16740E+00	0.16724E+00
70	NO2	0.17118E+00	0.17118E+00	0.17093E+00	0.17118E+00	0.17118E+00	0.17102E+00
71	NO3	0.17286E+00	0.17284E+00	0.17273E+00	0.17287E+00	0.17286E+00	0.17282E+00
72◇*	CCO_O2	0.20829E−01	0.20830E−01	0.21189E−01	0.20893E−01	0.20893E−01	0.21177E−01
73◇*	RCO_O2	0.45071E−01	0.45072E−01	0.45693E−01	0.45181E−01	0.45181E−01	0.45668E−01
74◇*	OH	−0.63646E−03	−0.63446E−03	0.38750E−02	0.67029E−03	0.67080E−03	0.38888E−02

Chemical species in the model are listed in KPP selected order. Non-reactive species in the model are marked with † and radicals are marked with ◇. A perturbation $\varepsilon = 1$ ppt was used in the finite difference approximation. For chemical species marked with * we used $\varepsilon = 0.001$ ppt.

24 h spin-up period $[t^s, t^0]$ is used to allow the concentrations to build up.

We performed the forward model integration with the ROS2 and RODAS3 solvers using an adaptive step size strategy as presented by Sandu et al. (1997). The tolerance for the local error in computing y^{i+1} is expressed as

$$\mathrm{Tol}_j = \mathrm{Atol} + \mathrm{Rtol} \times y_j^{i+1}, \quad 1 \leqslant j \leqslant n,$$

where Atol and Rtol represent a user-specified absolute and relative error tolerance. Tolerances may differ among the chemical species, but for simplicity we uniformly specified $\mathrm{Atol} = 1\ \mathrm{mol/cm^3}$ and $\mathrm{Rtol} = 10^{-3}$. Therefore, the integration error is mainly controlled by the relative error. The absolute tolerance will play a role in the step size selection only when Atol and $\mathrm{Rtol} \times y_j^{i+1}$ have the same order of magnitude, that is when some concentrations fell near the zero value. The results obtained with both integrators agree within the prescribed accuracy requirements. The evolution of the concentrations in the time interval $[t^0, t^0 + 120\mathrm{h}]$ is shown in Fig. 1 (reference run) for representative chemical species from the class of inorganics (O3, NO2, SO2), explicit (HCHO, CCHO, Ethene) and lumped (ALK4, OLE1, ARO1) organics, and in Fig. 2 (reference run) for the radicals OH, HO2, RO2_R.

2.2. Sparse linear algebra computations with KPP

For an efficient forward/adjoint integration the sparsity of the ODE system (1) associated with the chemical mechanism must be carefully exploited. The linear algebra computations required during the forward/adjoint integration are efficiently performed using KPP software. The dimension of the state vector of variable chemical species is $n = 74$, but the Jacobian matrix associated with the differential equations system has only 839 non-zero entries out of $74 \times 74 = 5476$ revealing a sparsity of about 85%. KPP selects an optimal ordering of the chemical species such that there are only 920 non-zero entries after the LU matrix decomposition. The KPP ordering of the variable chemical species in the model is presented in Table 1. Since the discrete adjoint model associated with Rosenbrock-type solvers requires Hessian matrices evaluation, it appears that a huge amount of memory must be allocated for Hessian storage. Taking advantage of the symmetry, the full Hessian matrices $H_i = \partial^2 f_i / \partial y^2$, $1 \leqslant i \leqslant n$ appear to require $74 \times 75 \times 37 = 205350$ entries to be stored. However, KPP analysis shows that the number of nonzero entries is NHESS = 838, which is less than 0.5% of the previous estimation. The KPP implementation of sparse linear algebra leads to significant computational savings and allows a very efficient forward/adjoint integration.

Table 2
Reference (E_i^{ref}), initial guess (E_i^{iguess}), and data assimilation (E_i^{assim}) estimated emission rates

Chemical species	Emission rate (ppm/min)				
	E_i^{ref}	E_i^{iguess}	$\lvert(E_i^{\text{ref}} - E_i^{\text{iguess}})/E_i^{\text{ref}}\rvert$	E_i^{assim}	$\lvert(E_i^{\text{ref}} - E_i^{\text{assim}})/E_i^{\text{ref}}\rvert$
NO	6.944E − 05	10.416E − 05	0.5	6.934E − 05	0.00130
NO2	3.472E − 05	5.208E − 05	0.5	3.474E − 05	0.00071
HONO	6.944E − 07	1.041E − 06	0.5	6.947E − 07	0.00053
SO2	3.472E − 05	5.208E − 05	0.5	3.462E − 05	0.00260
ETHENE	1.312E − 05	1.968E − 05	0.5	1.315E − 05	0.00238
ISOPRENE	3.007E − 07	4.510E − 07	0.5	3.007E − 07	0.00019
TERP	5.694E − 07	8.541E − 07	0.5	5.693E − 07	0.00005
MEOH	4.089E − 06	6.134E − 06	0.5	4.087E − 06	0.00060
HCHO	7.786E − 06	1.168E − 05	0.5	7.869E − 06	0.01059
CCHO	1.608E − 06	2.412E − 06	0.5	1.856E − 06	0.15447
RCHO	1.195E − 06	1.793E − 06	0.5	1.301E − 06	0.08800
GLY	8.431E − 08	1.264E − 07	0.5	9.072E − 08	0.07612
MGLY	5.815E − 08	8.722E − 08	0.5	6.497E − 08	0.11743
METHACRO	9.008E − 07	1.351E − 06	0.5	9.012E − 07	0.00044
ISOPROD	6.201E − 08	9.302E − 08	0.5	6.153E − 08	0.00780
BALD	5.217E − 08	7.825E − 08	0.5	5.356E − 08	0.02666
ACET	3.522E − 06	5.283E − 06	0.5	3.697E − 06	0.04974
MEK	2.264E − 06	3.397E − 06	0.5	2.372E − 06	0.04753
PROD2	1.340E − 06	2.010E − 06	0.5	1.352E − 06	0.00946
PHEN	4.206E − 07	6.310E − 07	0.5	4.207E − 07	0.00016
CRES	3.888E − 07	5.832E − 07	0.5	3.870E − 07	0.00452
ALK1	8.103E − 06	1.215E − 05	0.5	8.179E − 06	0.00938
ALK2	1.306E − 05	1.959E − 05	0.5	1.306E − 05	0.00049
ALK3	3.259E − 05	4.888E − 05	0.5	3.254E − 05	0.00126
ALK4	2.893E − 05	4.340E − 05	0.5	2.889E − 05	0.00165
ALK5	2.123E − 05	3.185E − 05	0.5	2.123E − 05	0.00033
ARO1	8.185E − 06	1.227E − 05	0.5	8.201E − 06	0.00202
ARO2	6.070E − 06	9.106E − 06	0.5	6.069E − 06	0.00021
OLE1	7.209E − 06	1.081E − 05	0.5	7.197E − 06	0.00165
OLE2	5.538E − 06	8.307E − 06	0.5	5.535E − 06	0.00048

3. Direct sensitivity calculations

We computed the direct sensitivities with respect to initial values and to rate coefficients using ROS2, RODAS3, and ROS4 integration methods. The accuracy of the results and the efficiency of the implementation are compared against a reference solution obtained with the direct-decoupled, off-the-shelf BDF code ODESSA (Leis and Kramer, 1986), with the tight tolerances Atol = 1e − 8 mol/cm^3, Rtol = 1e − 8.

Direct sensitivities of ozone concentration with respect to six rate coefficients are shown in Fig. 3.

ODESSA uses error control for both the concentrations and the sensitivities. We note that setting the proper values of the absolute tolerances for the sensitivities is difficult, since the sensitivity coefficients take values spanning a wide range of magnitudes. For this reason the KPP implementation of Rosenbrock methods only controls the concentration errors. The work-precision diagrams, i.e. the numerical errors versus the CPU time are presented in Fig. 4. The ozone concentration errors are shown in the left graphic. The errors of ozone sensitivity at final time with respect to all initial concentrations, i.e.

$$\text{ERR} = \sqrt{\frac{1}{n}\sum_{i=1}^{n}\left(\left.\frac{\partial \text{O}_3(t^{\text{F}})}{\partial y_i(t^0)}\right|_{\text{numeric}} - \left.\frac{\partial \text{O}_3(t^{\text{F}})}{\partial y_i(t^0)}\right|_{\text{reference}}\right)^2}$$

is shown in the right graphic. One notices that sensitivity coefficient errors are of the same order of magnitude as concentration errors. The errors in evaluating the sensitivities of the concentrations at the end of the simulation interval with respect to the initial ozone concentration, i.e.

$$\text{ERR} = \sqrt{\frac{1}{n}\sum_{i=1}^{n}\left(\left.\frac{\partial y_i(t^{\text{F}})}{\partial \text{O}_3(t^0)}\right|_{\text{numeric}} - \left.\frac{\partial y_i(t^{\text{F}})}{\partial \text{O}_3(t^0)}\right|_{\text{reference}}\right)^2}$$

are shown in the middle graphic. The results show that some sensitivities are solved inaccurately. Therefore, the concentrations-only error control strategy has to be carefully used. For ODESSA results were obtained by

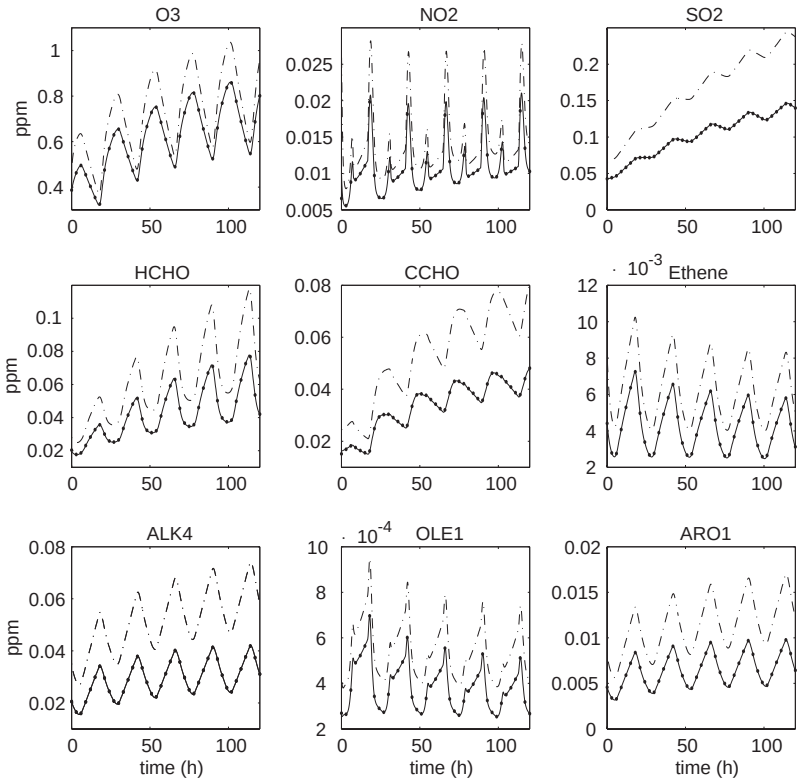

Fig. 1. Evolution of the concentrations for a 5 days forecast. Results are shown for chemical species representing the class of inorganics (O3, NO2, SO2), explicit (HCHO, CCHO, Ethene) and lumped (ALK4, OLE1, ARO1) organics. Reference run with continuous line, initial guess run with dashdot line, assimilation run with solid dots. Data assimilation is performed over a 24 h assimilation window [0,24]h.

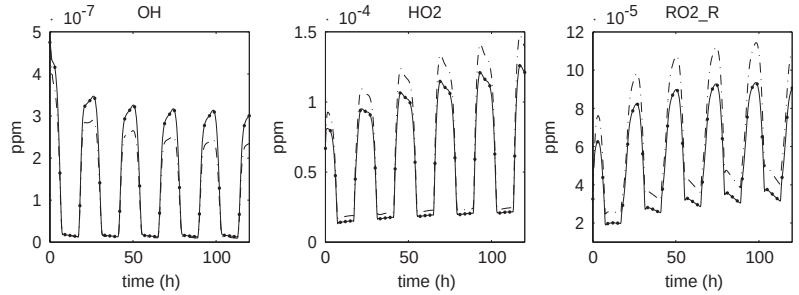

Fig. 2. Evolution of the concentrations of radical species OH, HO2, RO2_R for a 5 days forecast. Reference run with continuous line, initial guess run with dashdot line, assimilation run with solid dots. Data assimilation is performed over a 24 h assimilation window [0,24]h.

varying both the relative and absolute tolerances. The disappointing accuracies are presumably due to the fact that some of the sensitivity coefficients are extremely small (e.g. the sensitivities of radicals at final time with respect to the initial O_3 concentration), and consequently difficult to approximate.

The results of Fig. 4 also suggest that direct decoupled Rosenbrock methods are cost-effective (when compared to the BDF sparse code ODESSA) for providing sensitivities at low and medium accuracies. This conclusion parallels the fact that Rosenbrock methods are cost-effective for ODE integration (for calculating concentrations) in the low and medium accuracy range.

The computational times for the forward integration of the model, the direct-decoupled sensitivity with respect to all initial conditions and with respect to six

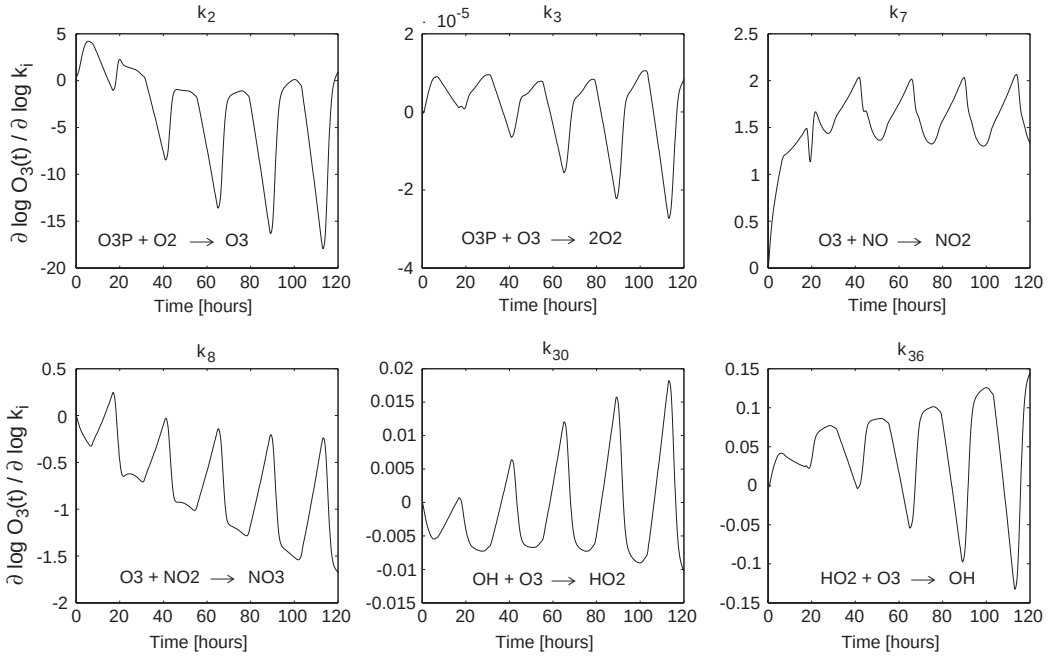

Fig. 3. The time evolution of $[O_3](t)$ direct sensitivity with respect to several rate coefficients.

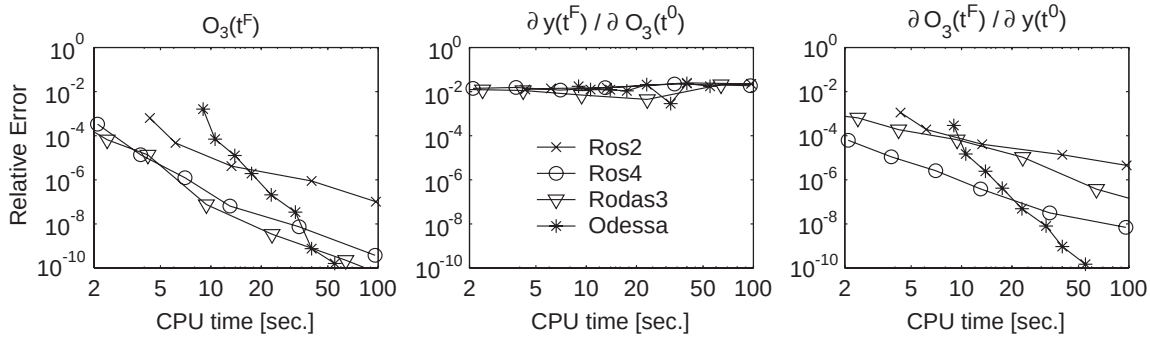

Fig. 4. The numerical errors versus CPU time for: $[O_3](t^F)$ (left), the direct sensitivity $\partial y(t^F)/\partial[O_3](t^0)$ (middle), and the direct sensitivity $\partial[O_3](t^F)/\partial y(t^0)$ (right).

rate coefficients are shown in Table 3. The ratios of DDM times to model integration times are sub-linear (about half the number of sensitivity coefficients) for sensitivity with respect to initial values. But these ratios are super-linear for the sensitivities with respect to rate coefficients. This can be explained by the overheads due to the analytical calculation of the function and Jacobian derivatives with respect to the rate coefficients.

4. Adjoint sensitivity analysis

In this section, we use the adjoint method to estimate the sensitivity of predicted ozone concentration $[O_3](t^F)$

Table 3
The CPU times (in seconds, on a Pentium III, 1 GHz) for the integration of the forward model, and the integration of the direct-decoupled system for sensitivities with respect to all initial values and with respect to six rate coefficients. Variable integration time stepping is employed. In parentheses are shown the ratios of DDM times to model integration times

Method	Model	DDM init. cond. (NVAR = 74)	DDM rate coeff. (NCOEFF = 6)
Ros2	1.87	73.60 (40)	11.01 (6)
Rodas3	0.66	25.54 (39)	10.36 (15)
Ros4	1.28	78.50 (61)	11.12 (9)
Odessa	2.23	87.82 (40)	21.57 (10)

at $t^F = t^0 + 120$h, first with respect to the initial conditions y^0, then with respect to the model state at intermediate instants in time $t^0 \leqslant t < t^F$, emissions and reaction rate coefficients. Issues related with validation of the model linearization, consistency between the discrete adjoint (DADJ) and continuous adjoint (CADJ) model, and accuracy of the evaluated gradients are addressed. A comparative study discrete versus continuous adjoint is presented. The computational expense of the adjoint model is analyzed in terms of memory storage requirements and CPU time relative to the forward model integration.

4.1. Adjoint model validation

The direct and the adjoint sensitivity methods provide first-order sensitivities that describe the linear response of the system with respect to variations in the model parameters. Since chemical reaction systems are nonlinear, the first problem to address is the validity of the linearization of model (1). For a given objective functional

$$g(p) = g(y(t^F, p)) \tag{2}$$

we will assume that the model linearization is satisfied and the evaluated sensitivity (gradient) $\nabla g(p) = \partial g/\partial p \in R^m$ is correct if the finite difference approximation

$$\frac{g(p + \varepsilon_i e_i) - g(p)}{\varepsilon_i} \approx \frac{\partial g(p)}{\partial p_i}, \quad 1 \leqslant i \leqslant m \tag{3}$$

is satisfactory for ε_i small enough. In the equation above, $e_i = (0, \ldots, 0, 1, 0 \ldots, 0)^T \in \Re^m$ is the unit vector in the ith direction of $\Re^m$.

Additional issues must be addressed for the adjoint model validation. Model (1) is nonlinear such that the adjoint model depends on the forward state evolution, which in turn depends on the parameter values. When variable step size integration is performed, the selected steps depend on the parameter values. For a valid test (3) there are two alternatives:

(i) perform a constant step size integration;
(ii) perform a variable step size integration to evaluate $g(p)$ and store the sequence of the steps taken. Then evaluate $g(p + \varepsilon_i e_i)$ using the same sequence of steps.

Using either (i) or (ii) we may perform a valid test for the *discrete adjoint* model which provides the sensitivity of the *numerically evaluated* response functional with respect to the model parameters. Since the forward model provides only approximate values of the continuum trajectory, the test (3) for the continuous adjoint gradients can only lead to an agreement within $O(\varepsilon) + O(\mathrm{Tol})$, where Tol represents the accuracy of the forward integration. We use a constant step size integration to validate the discrete adjoint model, then we show the consistency between the discrete and continuous adjoint models for an accurate variable step size forward/adjoint model integration.

4.1.1. Discrete adjoint model validation

We consider the ozone concentration at $t^F = t^0 + 120$h as the response functional, and the initial conditions as parameters. Therefore, $p = y^0$ and $g(y^0) = [O_3](t^F, y^0)$. Sensitivities are evaluated for a constant step size integration $h = 60$ s using ROS2 and RODAS3 solvers. For each solver we compare the discrete adjoint sensitivity against the finite difference approximation (3). Due to the wide range of concentrations, nonlinearity of the system and roundoff errors, finding an optimal perturbation ε for the finite difference approximation may be a difficult task requiring extensive trial and error experiments. We consider a perturbation in the initial conditions of 1 part-per-trillion (ppt) for each chemical species at a time, and perform $1 + 74$ runs for the finite difference approximation. For most of the chemical species an agreement of 4–6 significant digits is observed between the finite difference and the discrete adjoint gradients, which indicates that the adjoint gradients are properly evaluated. Sensitivity values using finite difference (FD) against discrete adjoint (DADJ) are presented in Table 1 for all chemical species and each numerical solver. In addition, the sensitivities obtained with the continuous adjoint model (CADJ) are also included in Table 1 for each solver. Note that the first eight chemical species in Table 1 are non-reactive and therefore their sensitivity values are zero. For some of the radical species (marked with * in Table 1), we used a perturbation of 10^{-3} ppt to obtain a satisfactory finite difference approximation. Only for the phenoxy radical (BZNO2_O) the finite difference approximation failed to provide reliable results. Since in our model the concentration of BZNO2_O is about 10^{-16} ppt, roundoff errors play a significant role in the finite difference estimate.

From Table 1 it can be seen that although in general we obtained close sensitivity values with different integrators, the accuracy of the forward integration may have a significant impact on the evaluated sensitivities. A good agreement between the finite difference approximation and the discrete adjoint evaluated sensitivities simply implies that the adjoint model was properly implemented. No indication is provided on how accurately we estimated *the true* sensitivities given by the exact solution of the forward/adjoint model. For some of the radical species and in particular, for the hydroxyl radical (OH) the discrete adjoint sensitivities we obtained with ROS2 and RODAS3 are quite different. These results indicate that the errors in computing the state evolution may be amplified through the differentiation of the numerical schemes. On another hand, the continuous adjoint

method applied for each solver offered a consistent sensitivity estimate and we obtained an accurate sensitivity value $\partial[O_3](t^F)/\partial[OH](t^0) = 0.003891$ with ODESSA package (see also Section 4.2) using the direct decoupled sensitivity method.

4.2. Accuracy of the adjoint sensitivities

We investigated the accuracy of the sensitivities evaluated with the continuous and discrete adjoint models. Reference sensitivity values were obtained by solving the ODE system (1) and the associated first-order parametric sensitivity equations using ODESSA code with $\mathrm{Rtol} = 10^{-6}$.

We begin our analysis by performing a fixed step size integration, $h = 60$ s of the forward/adjoint model using ROS2 and RODAS3 solvers and comparing the discrete and continuous adjoint sensitivities with the reference values obtained with ODESSA. A graphical illustration of the relative differences of the estimated sensitivity values is shown in Fig. 5.

For most components of the state vector, the discrete adjoint approach provided a more accurate sensitivity estimate than the continuous adjoint model. However, the continuous adjoint model provided more robust estimates, whereas large variations in the accuracy estimates may be observed for the discrete adjoint model. In particular, for some of the radical species (see e.g. TBU_O, $i_{\mathrm{TBU\_O}} = 22$, O3P, $i_{\mathrm{O3P}} = 58$, OH, $i_{\mathrm{OH}} = 74$ in Fig. 5 and also Table 1) the discrete adjoint estimate was not reliable while the continuous adjoint approach provided accurate values. To explain this behavior, we notice that the discrete adjoint model is induced by the forward integration and may be interpreted as a numerical method applied to the continuous adjoint model. Order reduction of the discrete adjoint for Runge–Kutta integration methods is investigated by Hager (2000). Sei and Symes (1995) show that stability and consistency properties are not always preserved by the discrete adjoint model and depend on the integration method.

Even for a modest accuracy of the model integration, a step size as small as a few seconds may be needed during the sunrise and sunset stiff transients. Since integration with a constant step of a few seconds may not be a practical approach, a variable step size integration with error control is desirable.

Variable step size numerical integration of the forward model (1) provides an estimate $\bar{y}(t^i)$ of the true solution $y(t^i)$, $\bar{y}(t^i) = y(t^i) + \delta y(t^i)$, and we may assume

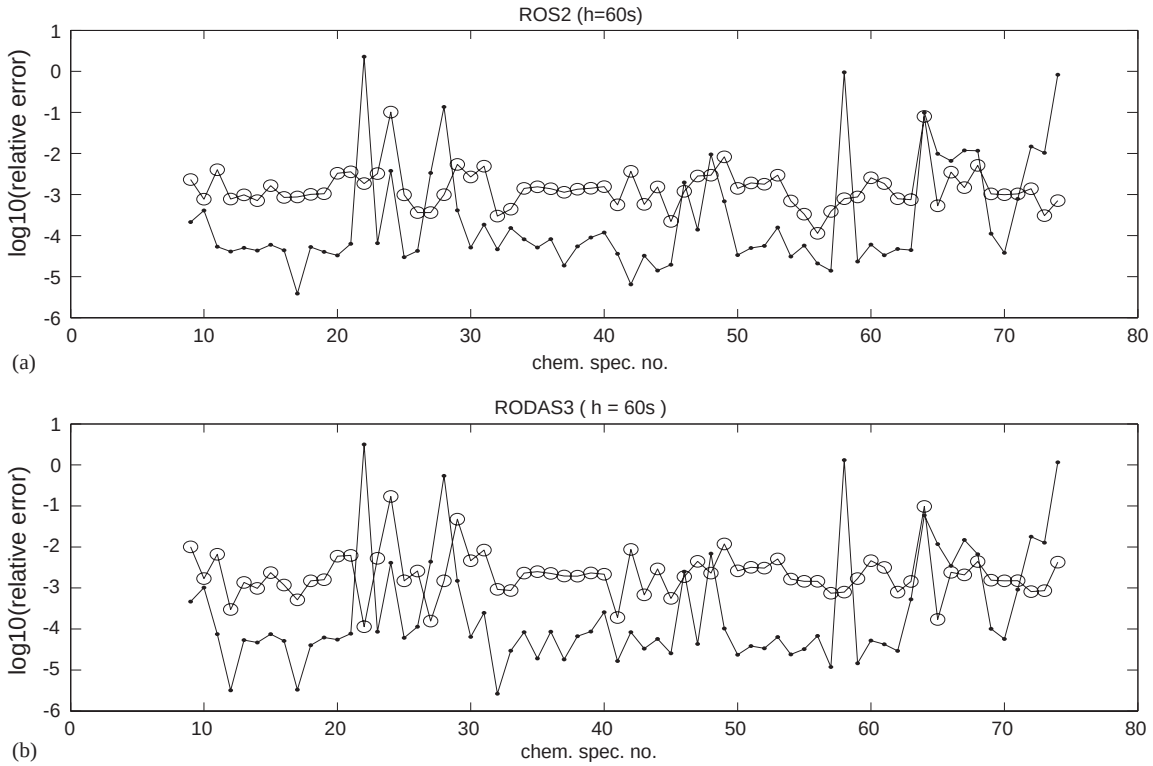

Fig. 5. Relative errors for the sensitivity values evaluated using the continuous (○) and discrete (.–) adjoint methods (a) for ROS2 and (b) for RODAS3, with a constant step size $h = 60$ s. The reference solution is obtained with ODESSA ($\mathrm{Rtol} = 10^{-6}$).

that the accuracy requirements of the forward integration are such that $\|\delta y(t^i)\| < \mathrm{Tol}$, where Tol is an user prescribed tolerance.

In the continuous adjoint approach we only have access to the approximate adjoint model

$$\frac{\mathrm{d}\lambda}{\mathrm{d}t} = -J^T(t, \bar{y}; p)\lambda, \tag{4}$$

$$\lambda(t^{\mathrm{F}}) = \frac{\partial g}{\partial y}(\bar{y}(t^{\mathrm{F}})), \tag{5}$$

which we attempt to solve numerically. If a forward model solution $\bar{y}(t^i)$ such that $\|\delta y(t^i)\| < \mathrm{Tol}$ is provided, by solving Eqs. (4)–(5) we may only obtain an estimate $\bar{\lambda} = \lambda + \delta\lambda$ with $\|\delta\lambda\| < C\,\mathrm{Tol}$ and the constant bound may be quite large. A judicious estimate of how the forward integration errors propagate into the adjoint model is difficult to obtain and significant insight may be gained through a second-order sensitivity analysis to evaluate $\partial\lambda/\partial y$. Such analysis is beyond the goal of this paper and we will consider a backward integration of the adjoint model (4)–(5) using the reversed sequence of steps taken during the forward integration.

The forward model (1) is integrated as in Section 2.1 with the tolerances $\mathrm{Atol} = 1\ \mathrm{mol/cm^3}$, $\mathrm{Rtol} = 10^{-3}$, using the variable step size ROS2 and RODAS3 solvers and reference sensitivity values are obtained with ODESSA.

We obtained accurate sensitivity values for both the continuous and discrete adjoint approach using the variable step size ROS2 and RODAS3 solvers. The results are presented in Fig. 6 for the RODAS3 integration and show a close agreement with the reference values obtained with ODESSA.

4.3. Time-dependent sensitivity analysis

The adjoint method provides an efficient tool for time-dependent sensitivity analysis. In this section the adjoint modeling is used to evaluate the sensitivity of ozone concentration $[O_3]$ at the end of the integration interval ($t^{\mathrm{F}} = t^0 + 120\mathrm{h}$) with respect to the model state at intermediate instants in time and emissions over the time interval $[t^1,\ t^{\mathrm{F}}]$, $t^0 \leqslant t^1 < t^{\mathrm{F}}$. Sensitivities with respect to constant and time-dependent reaction rates coefficients are also presented; they are obtained at minimal additional cost during the adjoint integration. We initialize the vector $\lambda(t) \in \mathscr{R}^n$ of the adjoint variables associated with the forward model (1) with $\lambda_j(t^{\mathrm{F}}) = 1$ for $j = O_3$ and zero for all other components.

4.3.1. Sensitivity to model state

VOC and NO_x chemistry initiated by reactions with hydroxyl (OH) and peroxy (RO2) radical species is essential to the ozone formation process. The impact on ozone concentration $[O_3](t^{\mathrm{F}})$ induced by variations in

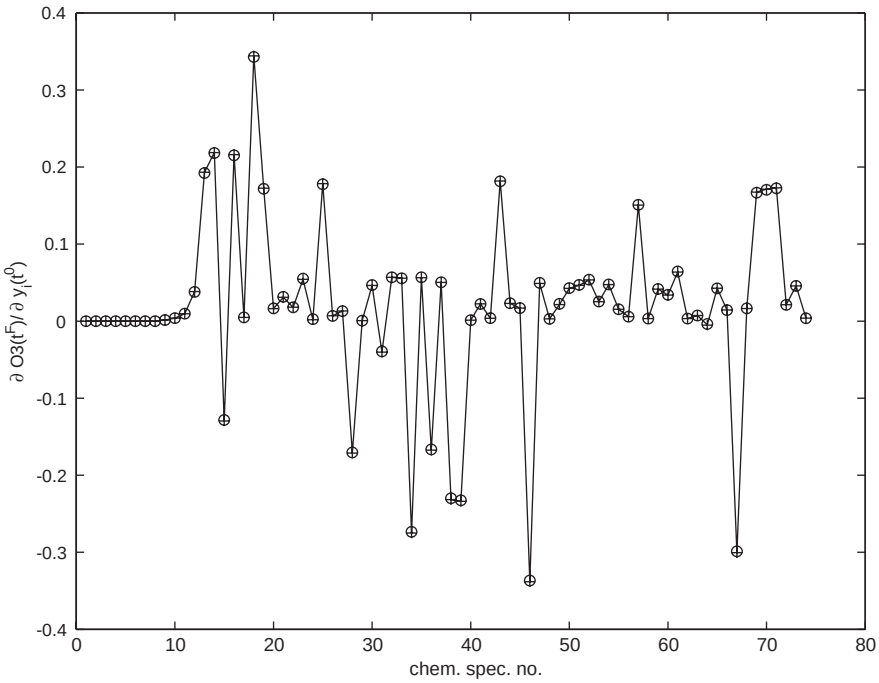

Fig. 6. Sensitivity values $\partial[O_3](t^{\mathrm{F}})/\partial y_i(t^0)$ obtained with ODESSA (−), discrete adjoint (+) and continuous adjoint (○) using variable step size RODAS3 integration.

the concentrations of the chemical species in the model at intermediate instants in time $t^0 \leqslant t < t^F$ may be analyzed by evaluating the time-dependent sensitivities

$$s_i(t) = \frac{\partial [O_3](t^F)}{\partial y_i(t)}, \quad 1 \leqslant i \leqslant n. \tag{6}$$

Using the adjoint model properties (Sandu et al., 2003), we identify $s_i(t) = \lambda_i(t)$ such that during the adjoint integration to obtain sensitivity with respect to the initial state $\lambda(t^0)$, we obtain at no additional cost the intermediate sensitivities (6). Due to the wide range of concentrations in the chemical system, we consider normalized sensitivity values given by the ratio

$$s_i^*(t) = \frac{\partial [O_3](t^F)}{\partial y_i(t)} \frac{y_i(t)}{[O_3](t^F)} = \frac{y_i(t)}{[O_3](t^F)} \lambda_i(t), \quad 1 \leqslant i \leqslant n, \tag{7}$$

which may be interpreted as the percentual change in the concentration $[O_3](t^F)$ due to 1% increase in the concentration of species i at moment t.

The adjoint integration provided the sensitivities of ozone with respect to all chemical species in the model and we obtained consistent estimates of $s_i^*(t)$, $t^0 \leqslant t < t^F$ within the prescribed accuracy range for both continuous and discrete adjoint approach using a variable step size integration.

Ozone formation is highly sensitive to the concentrations of NO_x species, as shown in Fig. 7. Increasing NO and NO2 concentrations result in increased ozone formation and the relative impact is highly dependent on the time of the day. Small relative sensitivities were obtained with respect to the radical species OH and HO2. Among the explicit reactive organic product species we found that the impact of variations in the formaldehyde (HCHO) and acetaldehyde (CCHO) concentrations were significant for the short time evolution of ozone concentrations. Among the lumped parameter species, a large relative sensitivity was obtained for lumped aldehydes (RCHO), alkanes with high OH reactivity (ALK4, ALK5), and aromatics (ARO1, ARO2). These results are also displayed in Fig. 7.

As a general remark, we notice that the sensitivity of ozone concentration at the end of the integration interval with respect to the state configuration during the previous 24 h is relatively large and it rapidly diminishes as time moves backward. Therefore, small

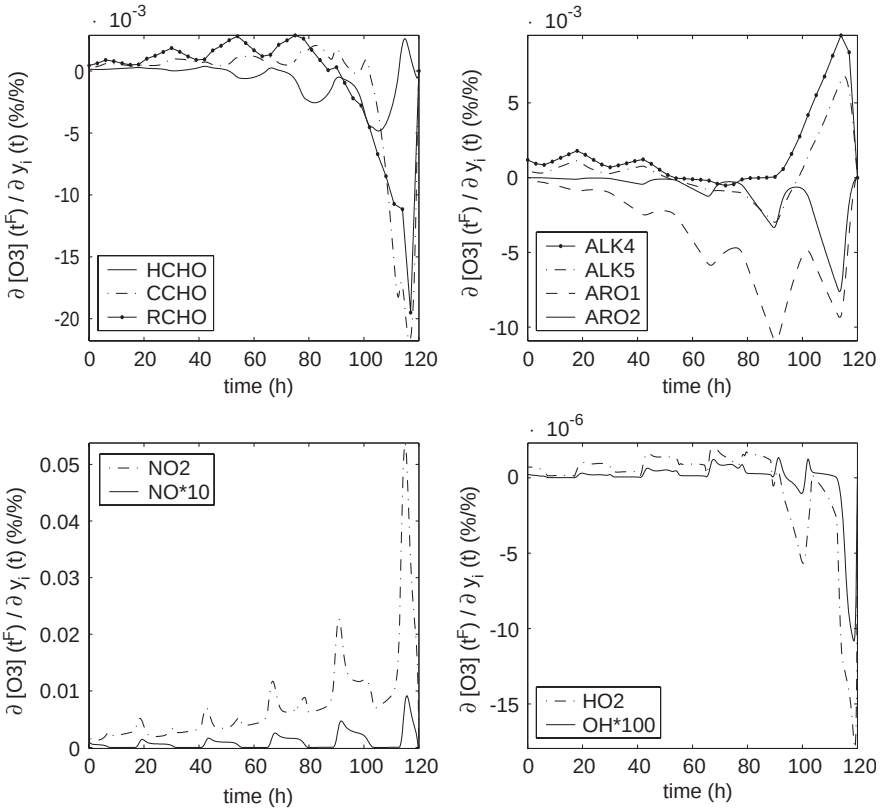

Fig. 7. Normalized $[O_3](t^F)$ sensitivity with respect to concentrations of several explicit and lumped organic species (top), NO_x, and the radicals OH and HO2 (bottom) at time t, $t^0 \leqslant t \leqslant t^F$.

variations in the concentrations during the first three days of the integration will have little influence on the ozone state at the end of the fifth day.

4.3.2. Sensitivity to emissions

The impact of various types of emitted VOC on ozone formation is given by the ozone reactivities of the VOC. The "incremental reactivity" (Carter, 1994) is given by the partial derivative of ozone with respect to the emissions of the VOC which represents the sensitivity of ozone to VOCs emissions. In this section we study the sensitivity of ozone concentration $[O_3]$ at the end of the integration interval ($t^F = t^0 + 120$h) with respect to NO_x and VOCs emissions over the time interval $[t^1, t^F], t^0 \leqslant t^1 < t^F$. In our model emissions are specified for 30 chemical species at a constant rate E_i as shown in Table 2 (E_i^{ref}) such that the total amount of pollutant i emitted in the time interval $[t^1, t^F]$ is given by

$$\mathscr{E}_i(t^1) = \int_{t^1}^{t^F} E_i(t)\,\mathrm{d}t = (t^F - t^1)E_i. \tag{8}$$

The sensitivities

$$s_i(\mathscr{E}, t^1) = \frac{\partial[O_3](t^F)}{\partial \mathscr{E}_i(t^1)} = \frac{1}{t^F - t^1}\int_{t^1}^{t^F} \lambda_i(t)\,\mathrm{d}t \tag{9}$$

may be evaluated *simultaneously* for all emission types using *a single* backward integration of the adjoint model. To derive Eq. (9) we used $\partial f_j/\partial E_i = 1$ if $i = j$, $\partial f_j/\partial E_i = 0$ if $i \neq j$ and the results in Section 3.1 in the companion paper Sandu et al. (2003). Normalized sensitivity values

$$s_i^*(\mathscr{E}, t^1) = s_i(\mathscr{E}, t^1)\frac{\mathscr{E}_i(t^1)}{[O_3](t^F)} \tag{10}$$

with respect to emissions of NO_x and lumped parameter species are shown in Fig. 8. Sensitivity values indicate that ozone formation will increase as NO_x and alkanes emissions increase, whereas increasing emissions of aromatics (ARO), alkenes (OLE) and terpenes (TERP) will inhibit ozone production.

As noted by Carter (1994), the incremental reactivity values are highly dependent on the scenario considered and we must emphasize that the results presented in this section are only valid for our particular scenario. Extensive testing is required before general conclusions may be drawn. A Monte Carlo analysis was used by Wang et al. (2000) for a SAPRC-97 chemical mechanism to study the uncertainties in incremental reactivity estimates for aromatic compounds.

4.3.3. Sensitivity to reaction rate coefficients

The adjoint method can be used to evaluate the sensitivity of ozone concentration $[O_3](t^F)$ with respect to reaction rate coefficients k_j. Chemical reactions in the model are written explicitly as

$$r_j: \quad \sum_{i=1}^{n} s_{i,j}^{-} y_i \xrightarrow{k_j} \sum_{i=1}^{n} s_{i,j}^{+} y_i, \quad 1 \leqslant j \leqslant R, \tag{11}$$

where $s_{i,j}$ are the stoichiometric coefficients. We distinguish between the sensitivity with respect to thermal reactions rate coefficients which in our model are maintained constant, and sensitivity with respect to the photolytical reactions rates which are time dependent.

The sensitivity with respect to constant reaction rates k_j are expressed as

$$s_j(t^1) = \int_{t^1}^{T} \left(\frac{\partial f}{\partial k_j}\right)^T \lambda\,\mathrm{d}t, \quad t^0 \leqslant t^1 \leqslant t^F, \tag{12}$$

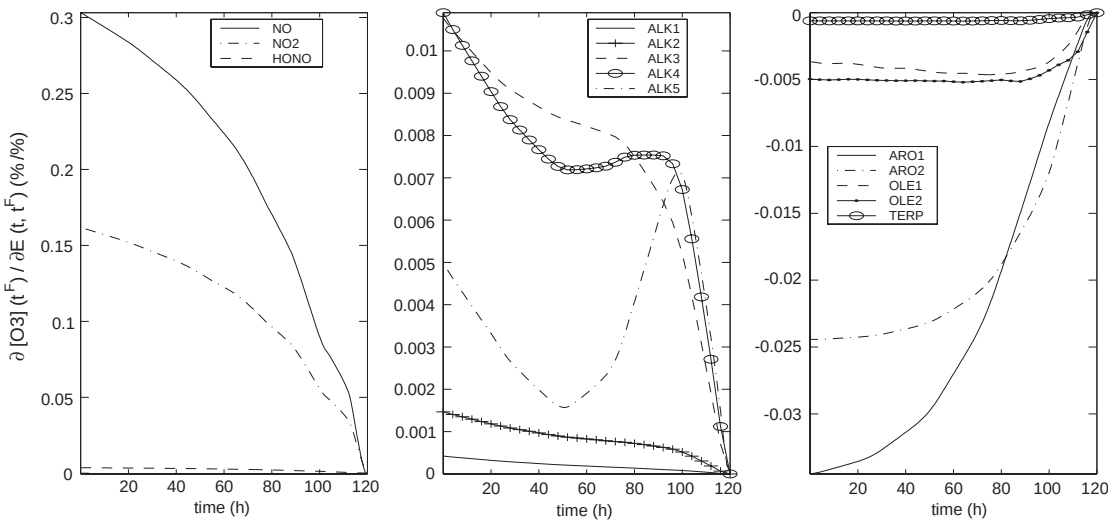

Fig. 8. Normalized $[O_3](t^F)$ sensitivity with respect to NO_x emissions and lumped parameter species emissions in the time interval $[t, t^F]$, $t^0 \leqslant t < t^F$.

where

$$\frac{\partial f_i}{\partial k_j} = (s^+_{i,j} - s^-_{i,j}) \prod_{i=1}^{n} y_i^{s^-_{i,j}} \tag{13}$$

and λ is the vector of adjoint variables associated with the state vector y. We used the trapezoidal rule to evaluate the right-hand side integrals in Eq. (12) and normalized sensitivity values

$$s^*_j(t^1) = s_j(t^1) \frac{k_j}{[O_3](t^F)} \tag{14}$$

with respect to few of the significant reactions in ozone chemistry are shown in Fig. 9.

Sensitivity with respect to instantaneous changes in the photolysis rates $k_j(t)$ at time t^1 are given by

$$s_j(t^1) = \left(\frac{\partial f}{\partial k_j}\right)^T \lambda|_{t=t^1}, \quad t^0 \leqslant t^1 \leqslant t^F. \tag{15}$$

In Fig. 10 we show the normalized sensitivity values (15) with respect to the photolysis rates that proved to be most significant in ozone formation.

4.4. Computational aspects

The implementation, accuracy, and efficiency of the decoupled-direct method (DDM) for sensitivity analysis in a three-dimensional air quality model are analyzed in detail by Dunker et al. (2002b). In their study Dunker et al. (2002b) show that the efficiency of the DDM (measured as CPU time per sensitivity parameter) improves as the number of model parameters increases.

The computational expense of the adjoint method is given by the memory resources that need to be allocated for storage of the forward model state time series and the CPU time of the gradient evaluation. Anticipating applications to large-scale transport-chemistry models in an operator splitting environment, KPP implements a two-level checkpointing scheme to store the forward model state evolution. The integration interval $[t^0, t^F]$ is uniformly divided in subintervals of length $dt: \mathscr{I}^i_{\rightarrow} = [t^i, t^{i+1}]$, $1 \leqslant i \leqslant I$. The interval length dt is specified by the user, in our experiments $dt = 15$ min. A first forward run from t^0 to t^F is used to store the model state at the end of each interval $\mathscr{I}^i_{\rightarrow}$, such that an array of dimension $n \times I$ is stored at this stage. Adjoint (backward) integration in the interval $\mathscr{I}^i_{\leftarrow} = [t^{i+1}, t^i]$, $i = I, 1, -1$ includes a second forward integration in $\mathscr{I}^i_{\rightarrow}$ to store the model state after each integration step h^i_j in the $\mathscr{I}^i_{\rightarrow}$ interval. For variable step size integration the sequence of steps taken $\{h^i_j\}$ needs also to be stored. The pure adjoint (backward) integration is then performed in the interval $\mathscr{I}^i_{\leftarrow}$ and may require some additional forward recomputations of the internal stages of the numerical method at each step. Therefore, the gradient evaluation requires two full forward runs and the pure backward integration. For the 5 days integration with the accuracy $Atol = 1$ mol/cm^3, $Rtol = 10^{-3}$, ROS2 required 9970 steps, whereas RODAS3 required only 5115. However, per step RODAS3 is more expensive

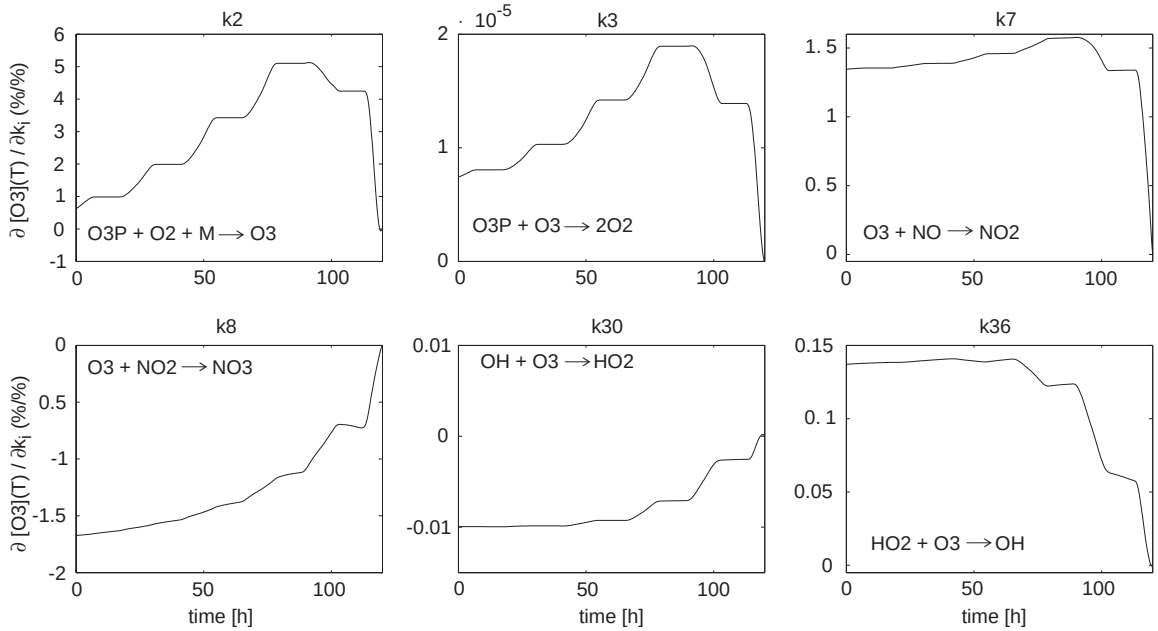

Fig. 9. Normalized $[O_3](t^F)$ sensitivity with respect to constant reaction rate coefficients.

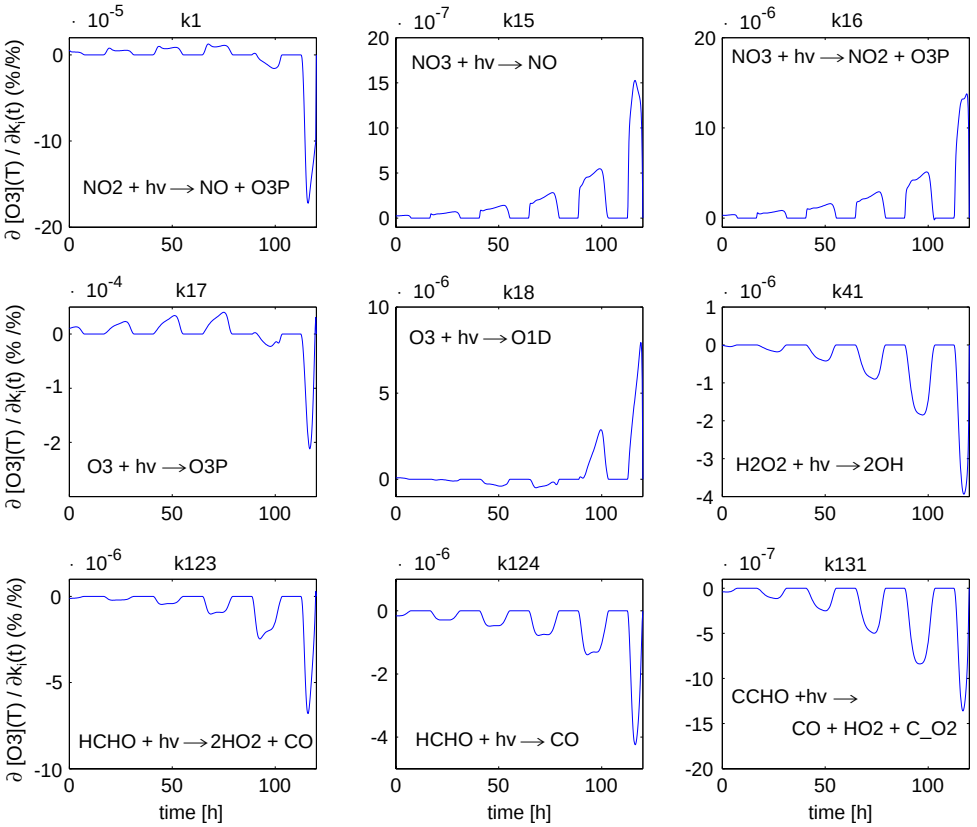

Fig. 10. Normalized $[O_3](t^F)$ sensitivity with respect to photolysis rate coefficients at time t.

Table 4
CPU time (in seconds) of the forward and adjoint integration with a constant step size $h = 60$ s

Numerical method	CPU time (s)						
	FWD	CADJ	$(\nabla g)_{CADJ}$	$(\nabla g)_{CADJ}$/FWD	DADJ	$(\nabla g)_{DADJ}$	$(\nabla g)_{DADJ}$/FWD
RODAS3	0.91	1.0 8	3.00	3.29	2.10	4.02	4.41
ROS2	0.74	0.81	2.39	3.23	1.40	2.98	4.03

The gradient time ∇g includes two forward model integrations (FWD), the pure discrete (and respectively continuous) adjoint integration DADJ (CADJ), and additional overhead due to trajectory save/load. Experiments performed on a Pentium III, 1 GHz.

since it has four internal stages, whereas ROS2 has only two.

Griewank (2000) has shown that the computational cost of the discrete adjoint code CPU(DADJ) is of the same order as the computational cost of the forward model integration CPU(FWD) (bounded by a factor 5 if no restrictions are considered on the memory access time). Neglecting the CPU time of the forward recomputations, for the continuous adjoint model a ratio CPU(CADJ)/CPU(FWD) ~ 1 is desirable using the same numerical method in both the forward and backward integrations. The CPU time required by the pure continuous (CADJ), discrete (DADJ) adjoint integrations, and gradient evaluation (∇g) versus the CPU time of the forward integration (FWD) is shown in Table 4 for ROS2 and RODAS3 integrators using a constant step size forward/backward integration with $h = 60$ s. The total CPU time required for gradient evaluation CPU(∇g) includes two forward runs, adjoint integration and the additional overhead introduced by the forward state time series storage/reload. The results indicate that very efficient implementations for both discrete and continuous adjoint models are obtained using KPP software.

4.4.1. On the applicability of the direct and adjoint sensitivity methods

The integration of the direct and adjoint sensitivity models provides complementary information. In the direct approach, the sensitivities of all concentrations with respect to one parameter, e.g. $\partial y(t^F)/\partial y_j(t^0)$, may be obtained by integrating one additional n-dimensional sensitivity equation. During this integration the derivatives $\partial y(t)/\partial y_j(t^0)$, $t^0 < t < t^F$ *of the time-varying concentrations* are also obtained at no additional cost. In the adjoint approach, the sensitivity of an objective functional with respect to all model parameters, e.g. $\partial O_3(t^F)/\partial y(t^0)$, may be obtained using a single computational run of the n-dimensional adjoint model. During this integration, the derivatives *with respect to the time varying concentrations* $\partial O_3(t^F)/\partial y(t)$, $t^0 < t < t^F$ are also obtained at no additional cost.

In the direct sensitivity approach the computational cost increases with the number of parameters, whereas in the adjoint approach the computational cost increases with the number of objective functionals. From this point of view, the adjoint method is particularly suitable for large-scale variational data assimilation applications where the sensitivity (gradient) of a scalar cost functional must be computed. The results presented in Tables 3 and 4 provide insight on the efficiency of the direct and adjoint methods for gradient evaluation. One should notice that while the results for the direct-decoupled method are presented for a variable step size integration, the results for the adjoint method are presented for a constant step size ($h = 60$ s) integration. Therefore, the absolute CPU time does not provide a valid measure for comparison. As a measure of efficiency, we consider the ratio between the CPU time to obtain the sensitivities and the CPU time of the forward model integration. While the ratios obtained with the direct-decoupled method range from 39 to 61, the adjoint method provided the gradient at a ratio between 3 (continuous adjoint) and 4.5 (discrete adjoint). These results show that the adjoint modeling is a more efficient approach to evaluate the sensitivity of a scalar response function with respect to a large number of input parameters.

Seefeld and Stockwell (1999) showed how the decoupled direct method (DDM) may be used to provide sensitivities with respect to time dependent parameters. For comprehensive three-dimensional air quality models, the DDM has been successfully applied by Dunker et al. (2002a, b) to obtain sensitivities of the model output with respect to a relatively small number of parameters ($\sim 10^2$). Dominguez and Russell (2000) use DDM to perform a four-dimensional data assimilation for emissions estimates. The adjoint method has been proved to be a feasible tool for large-scale ($\sim 10^6$ parameters) chemical data assimilation (Elbern and Schmidt, 1999; Errera and Fonteyn, 2001).

5. Applications to variational data assimilation

Adjoint modeling is an essential tool for large-scale variational data assimilation applications. The variational methods have been extensively used in data assimilation for meteorological and oceanographical models and show promising results for atmospheric chemistry applications (Fisher and Lary, 1995; Elbern and Schmidt, 1999; Errera and Fonteyn, 2001). Four-dimensional variational data assimilation (4D-Var) searches for an optimal set of model parameters which minimizes the discrepancies between the model forecast and time distributed observational data over the assimilation window. A practical implementation of the minimization process requires a fast and accurate evaluation of the gradient of the cost functional which may be provided by adjoint modeling.

In meteorological applications variational techniques are mostly used to find an optimal initial state of the model ($p = y^0$). In atmospheric chemistry modeling uncertainties in various model input parameters (e.g. emission rates, boundary values) must be also considered. For an in-depth analysis of the parameter estimation, identifiability issues and regularization techniques in the context of inverse modeling we will refer to Tarantola (1987). A review of the use of the adjoint method in four-dimensional atmospheric chemistry data assimilation is presented by Wang et al. (2001). In this section we investigate the ability of the 4D-Var technique to retrieve the initial model state and provide accurate emission estimates using observational data information. We briefly outline a discrete 4D-Var problem formulation and we will refer to Jazwinski (1970) and Daley (1991) for a complete description of the various assumptions used by the data assimilation techniques and the probabilistic interpretation. The numerical experiments are performed using the ROS2 solver with variable step size and a discrete adjoint model.

5.1. Data assimilation framework

The data assimilation procedure is set using the twin experiments method as follows:

Reference run: we start a model run at local noon $t^s = 12{:}00$LT with the concentration of all variable chemical species set to zero and the ''reference'' emission rates E_i^{ref} shown in Table 2. The model state obtained after a 24 h run at $t^0 = t^s + 24$h is considered as reference (''true'') initial state $(y^0)^{ref}$ of the model for a 5 days reference run $[t^0, t^0 + 120\text{h}]$.

Initial guess run: the experiment is repeated with emission rates increased by 50%, $E_i^{iguess} = 1.5E_i^{ref}$, as shown in Table 2. The model state obtained after a 24 h run at $t^0 = t^s + 24$h is considered as ''initial guess''

model state for a 5 days forecast run using E_i^{iguess} as emission rates.

Observations and assimilation window: We consider a 24 h assimilation window $[t^0, t^0 + 24\text{h}]$. No observations are provided for radical species (marked with $\diamond$ in Table 1). For all other chemical species in the model concentrations obtained during the reference run are provided as hourly observations $\bar{y}_i^k$ starting from $t^0 + 1\text{h}$.

Parameters: the control parameters are the concentration of variable chemical species at t^0 (dimension 74) and the emission rates (dimension 30), $p = (y^{0T}, E^T)^T$.

Cost functional: We assume that information to the data assimilation process is provided only by the "observations" such that no background term is included in the cost functional. To achieve a better scaling and to eliminate the positivity constraint, we consider $\ln p$ as control variables and the logarithmic form of the cost functional

$$\mathcal{J}(\ln p) = \frac{1}{2}\sum_{k=1}^{24}\sum_{i\in\mathcal{O}^k}[\ln y_i^k - \ln \bar{y}_i^k]^2, \tag{16}$$

where $\mathcal{O}_k$ represents the set of components of the state vector observed at t^k.

Optimization algorithm: Quasi-Newton limited memory L-BFGS (Byrd et al., 1995). The optimization proceeds until the cost functional is reduced to 0.01% of its initial value.

5.2. Numerical results

Using data assimilation we aim to provide an accurate estimate of the true initial model state $(y^0)^{\text{ref}}$ and emission rates E_i^{ref} such that an improved forecast is obtained for a 5 days model run. In the data assimilation process information provided by the observations is propagated to all the variables of the model. Chemical interactions among the model variables may allow the assimilation process to provide an improved forecast not only for the observed components of the state vector, but also for the chemical species for which observations are not available. Therefore, we further investigate the ability of the data assimilation to provide an accurate estimate of the evolution of the concentrations of radical species for which no observations were provided.

The reference run, the initial guess forecast, the assimilation results and the forecast after the assimilation process takes place are shown in Figs. 1 and 2 for various chemical species. By performing data assimilation, not only we have obtained an accurate representation of the model state evolution in the assimilation window [0,24]h, but also an accurate forecast was obtained for the full five days period. An accurate evolution of the concentrations of the radical species was also obtained. Emission rates estimates E_i^{assim} displayed in Table 2 show that using data assimilation the true emission rate values were successfully retrieved. We notice that not all parameters were estimated with the same accuracy (see e.g., TERP and Isoprene vs. CCHO and MGLY) which shows that the assimilation procedure would benefit from a better scaling (weighting) of the cost functional components. Dominguez and Russell (2000) analyzed the impact of several weighting schemes in four-dimensional data assimilation to adjust emissions inventories to observational data.

6. Conclusions and future work

In this paper, we presented an extensive set of numerical experiments and applications of the new Kinetic PreProcessor release KPP-1.2 to direct decoupled and adjoint sensitivity analysis. Our results indicate that KPP may be used as a flexible and efficient tool to generate code for sensitivity studies of the chemical reactions mechanisms. We illustrated KPP abilities by selecting a challenging test model, the state-of-the-science gas-phase chemical mechanism SAPRC-99. For this comprehensive model implementation of the direct-decoupled sensitivity method and hand generation of the adjoint code may be a difficult, time consuming, and error prone task.

Issues related with model linearization, accuracy, consistency, and computational expense of the discrete and continuous adjoint model were addressed. The new direct-decoupled Rosenbrock methods we proposed have been shown to be cost-effective for providing sensitivities at low and medium accuracies. In addition, particular properties of the Rosenbrock methods may be exploited for the adjoint modeling (Daescu et al., 2000). By taking full advantage of the sparsity of the chemical mechanism, the KPP software generates efficient discrete and continuous adjoint models.

Our comparative study shows that the continuous adjoint model offers more flexibility, is computationally less expensive, and may provide more robust results than the discrete adjoint model. Implementation of a discrete adjoint model is more suitable for data assimilation applications since the provided gradient is exact relatively to the evaluated cost functional.

We should emphasize that the efficiency of the KPP software relies on its particular design for chemical kinetics systems and KPP is not a general purpose adjoint modeling tool as TAMC (Giering and Kaminski, 1998) or Odyssée (Rostaing et al., 1993). Generating the discrete adjoint model associated with sophisticated numerical integrators is a complex task and an efficient implementation requires in-depth knowledge of the numerical scheme and forward mode computations. For this reason, the use of discrete adjoints in atmospheric chemistry applications has been limited to

explicit or low order linearly implicit numerical methods. For efficiency, a hand generated discrete adjoint code was often implemented (Elbern and Schmidt, 1999). Currently, KPP provides discrete adjoint implementation of the linearly implicit Euler, ROS2, and RODAS3 solvers, whereas the continuous adjoint model may be integrated with any user selected numerical method. As our research advances, new solvers from the class of Runge–Kutta methods will be included in discrete adjoint mode.

Adjoint modeling has various applications and few of them were illustrated in this paper: backward sensitivity analysis, parameter estimation, and data assimilation. Model reduction of chemical kinetics is an important field which we will investigate in our future work using direct/adjoint sensitivity analysis. By providing efficient operations involving Hessian matrices, KPP software may be also used to obtain second order information which may be applied to sensitivity analysis and data assimilation (Le Dimet et al., 2002).

An efficient implementation of the chemistry module into comprehensive 3D air quality models is essential as computations involving chemical transformations may require as much as 90% of the total CPU time. Applications of the adjoint method to atmospheric chemistry represent a new research direction which is growing at a fast pace and the KPP software may be used to facilitate the direct/adjoint model integration.

Acknowledgements

The authors are grateful to NSF support for this work through the award ITR AP&IM-0205198. The work of A. Sandu was also supported in part by the NSF CAREER award ACI-0093139. D.N. Daescu acknowledges the support from the Supercomputing Institute for Digital Simulation and Advanced Computation of the University of Minnesota.

References

Aiken, R.C. (Ed.), 1985. Stiff Computation. Oxford University Press, Oxford.

Byrd, R.H., Lu, P., Nocedal, J., 1995. A limited memory algorithm for bound constrained optimization. SIAM Journal on Scientific Computing 16 (5), 1190–1208.

Carmichael, G.R., Peters, L.K., Kitada, T., 1986. A second generation model for regional-scale transport/chemistry/deposition. Atmospheric Environment 20, 173–188.

Carter, W.P.L., 1994. Development of ozone reactivity scales for volatile organic compounds. Journal of the Air and Waste Management Association 44, 881–899.

Carter, W.P.L., 2000a. Implementation of the SAPRC-99 chemical mechanism into the models-3 framework. Report to the United States Environmental Protection Agency, January 2000.

Carter, W.P.L., 2000b. Documentation of the SAPRC-99 chemical mechanism for VOC reactivity assessment. Final Report to California Air Resources Board Contract No. 92-329, and 95-308, May 2000.

Daescu, D., Carmichael, G.R., Sandu, A., 2000. Adjoint implementation of Rosenbrock methods applied to variational data assimilation problems. Journal of Computational Physics 165 (2), 496–510.

Daley, R., 1991. Atmospheric Data Analysis. Cambridge University Press, Cambridge, 457pp.

Damian-Iordache, V., Sandu, A., Damian-Iordache, M., Carmichael, G.R., Potra, F.A., 2002. The kinetic preprocessor KPP—a software environment for solving chemical kinetics. Computers and Chemical Engineering 26 (11), 1567–1579.

Dominguez, A.M., Russell, A.G., 2000. Iterative inverse modeling and direct sensitivity analysis of a photochemical air quality model. Environmental Science and Technology 34, 4974–4981.

Dunker, A.M., Yarwood, G., Ortmann, J.P., Wilson, G.M., 2002a. Comparison of source appointment and source sensitivity of ozone in a three-dimensional air quality model. Environmental Science and Technology 36, 2953–2964.

Dunker, A.M., Yarwood, G., Ortmann, J.P., Wilson, G.M., 2002b. The decoupled direct method for sensitivity analysis in a three-dimensional air quality model—implementation, accuracy, and efficiency. Environmental Science and Technology 36, 2965–2976.

Elbern, H., Schmidt, H., 1999. A four-dimensional variational chemistry data assimilation scheme for Eulerian chemistry transport model. Journal of Geophysical Research 104 (D15), 18583–18598.

Errera, Q., Fonteyn, D., 2001. Four-dimensional variational chemical assimilation of CRISTA stratospheric measurements. Journal of Geophysical Research 106 (D11), 12253–12265.

Fisher, M., Lary, D.J., 1995. Lagrangian four-dimensional variational data assimilation of chemical species. Quarterly Journal of the Royal Meteorological Society 121, 1681–1704.

Giering, R., Kaminski, T., 1998. Recipes for adjoint code construction. ACM Transactions on Mathematical Software 24 (4), 437–474.

Griewank, A., 2000. Evaluating derivatives: Principles and Techniques of Algorithmic Differentiation. Frontiers in Applied Mathematics, Vol. 19. SIAM, Philadelphia.

Hager, W.W., 2000. Runge–Kutta methods in optimal control and the transformed adjoint system. Numerische Mathematik 87, 247–282.

Hairer, E., Wanner, G., 1991. Solving Ordinary Differential Equations II. Stiff and Differential-Algebraic Problems. Springer, Berlin.

Jazwinski, A.H., 1970. Stochastic Processes and Filtering Theory. Academic Press, New York, NY.

Le Dimet, F.-X., Navon, I.M., Daescu, D.N., 2002. Second order information in data assimilation. Monthly Weather Review 130 (3), 629–648.

Leis, J.R., Kramer, M.A., 1986. ODESSA—an ordinary differential equation solver with explicit simultaneous sensitivity analysis. ACM Transactions on Mathematical Software 14 (1), 61–67.

Lutz, A.E., Kee, R.J., Miller, J.A., 1987. SENKIN: a fortran program for predicting homogeneous gas phase chemical kinetics with sensitivity analysis. Sandia Report #SAND87-8248; Sandia National Laboratories.

Radhakrishnan, K., 2003. LSENS: Multipurpose kinetics and sensitivity analysis code for homogeneous gas-phase reactions. AIAA Journal 41 (5), 848–855.

Rostaing, N., Dalmas, S., Galligo, A., 1993. Automatic differentiation in Odyssée. Tellus 45, 558–568.

Sandu, A., Blom, J.G., Spee, E., Verwer, J.G., Potra, F.A., Carmichael, G.R., 1997. Benchmarking stiff ODE solvers for atmospheric chemistry equations II—Rosenbrock Solvers. Atmospheric Environment 31, 3459–3472.

Sandu, A., Daescu, D.N., Carmichael, G.R., 2003. Direct and adjoint sensitivity analysis of chemical kinetic systems with KPP: I—theory and software tools. Atmospheric Environment, this issue, doi:10.1016/j.atmosenv.2003.08.019

Seefeld, S., Stockwell, W.R., 1999. First-order sensitivity analysis of models with time-dependent parameters: an application to PAN and ozone. Atmospheric Environment 33, 2941–2953.

Sei, A., Symes, W.W., 1995. A note on consistency and adjointness for numerical schemes. Technical Report 95527, Department of Computational and Applied Mathematics, Rice University, Houston, TX.

Tarantola, A., 1987. Inverse Problem Theory: Methods for Data Fitting and Model Parameter Estimation. Elsevier Science Publishers, New York, NY.

Verwer, J.G., Spee, E., Blom, J.G., Hunsdorfer, W., 1999. A second order Rosenbrock method applied to photochemical dispersion problems. SIAM Journal on Scientific Computing 20, 1456–1480.

Wang, L., Milford, J.B., Carter, W.P.L., 2000. Reactivity estimates for aromatic compounds. Part 2. Uncertainty in incremental reactivities. Atmospheric Environment 34, 4349–4360.

Wang, K.Y., Lary, D.J., Shallcross, D.E., Hall, S.M., Pyle, J.A., 2001. A review on the use of the adjoint method in four-dimensional atmospheric-chemistry data assimilation. Quarterly Journal of the Royal Meteorological Society 127 (576 (Part B)) 2181–2204.